Atmos. Chem. Phys. Discuss., https://doi.org/10.5194/acp-2018-260
Manuscript under review for journal Atmos. Chem. Phys.
Discussion started: 26 March 2018

Atmospheric Chemistry and Physics Discussions

Errors in Nanoparticle Growth Rates Inferred from Measurements in Chemically Reacting Aerosol Systems

Chenxi Li[1] and Peter H. McMurry[1]

[1]Department of Mechanical Engineering, University of Minnesota, Minneapolis, MN, 55455, USA

Correspondence to: Chenxi Li (lixx3838@umn.edu)

Abstract. In systems where aerosols are being formed by chemical transformations, individual particles grow due to the addition of molecular species. Efforts to improve our understanding of growth often focus on attempts to reconcile observed growth rates with values calculated from models. However, because it is typically not possible to measure the growth rates of individual particles in chemically reacting systems, they must be inferred from measurements of aerosol properties such as size distributions, particle number concentrations, etc. This work quantifies errors in growth rates obtained using methods that are commonly employed for analyzing atmospheric data. We analyze "data" obtained by simulating the formation of aerosols in a system where a single chemical species is formed at a constant rate, R. We show that the maximum possible error in measured growth rates occurs for collision-controlled nucleation in a single-component system in the absence of a pre-existing aerosol, wall losses, evaporation or dilution, as this leads to the highest concentrations of nucleated particles. Those high concentrations lead to high coagulation rates that cause the nucleation mode to grow faster than would be caused by vapor condensation alone. We also show preexisting particles, when coupled with evaporation, can significantly decrease the concentration of nucleated particles. This leads to decreased discrepancies between measured growth rate and true growth rate by reducing coagulation. Conversely, the same concentration of preexisting particles has much less effect on growth rates during collision-controlled nucleation.

Atmos. Chem. Phys. Discuss., https://doi.org/10.5194/acp-2018-260
Manuscript under review for journal Atmos. Chem. Phys.
Discussion started: 26 March 2018

Atmospheric Chemistry and Physics Discussions

1 Introduction

Aerosol systems undergo transformations by processes that include coagulation, convection, deposition on surfaces, source emissions, nucleation, growth, etc. The aerosol general dynamic equation (GDE) (Friedlander, 2000;Gelbard and Seinfeld, 1979, 1980) describes the time rate of change of size-dependent particle concentration and composition by such processes.

Growth involves changes in the size of individual particles due to the addition or removal of molecular species. While most work to date has focused on condensation and evaporation, chemical processes such as acid-base reactions, organic salt formation, liquid phase reactions, and the accretion of two or more organic molecules to form a larger compound having lower volatility may also contribute to growth (McMurry and Wilson, 1982;Riipinen, 2012;Lehtipalo 2014). In a chemically reacting system, the total diameter growth rate, *GR*, is given by the sum of all such processes:

$$\frac{dd_p}{dt} = GR = GR_{condensation-evaporation} + GR_{acid-base\ reactions} + GR_{accretion} + GR_{other}. \quad (1)$$

The effect of growth on the aerosol distribution function is given by (Heisler and Friedlander, 1977):

$$\left.\frac{\partial n}{\partial t}\right|_{Growth} = -\frac{\partial}{\partial d_p}\left[n(d_p,t)\frac{dd_p}{dt}\right], \quad (2)$$

where the aerosol number distribution, $n(d_p,t)$ is defined such that the number concentration of particles between d_p and $d_p + dd_p$ is equal to $n(d_p,t)dd_p$. Coagulation, including the coagulation of a molecular cluster with a larger particle, can also lead to particle growth. It is worthwhile, however, to treat coagulation and growth separately. Coagulation is accounted for with the coagulation integrals in the GDE and is a relatively well understood process that can be described with reasonable confidence in models. Growth involves processes that are not well understood for chemically complex aerosol systems, such as the atmosphere.

Progress towards understanding growth can be achieved through efforts to reconcile GRs that are observed experimentally with values predicted by models. Such work requires that size- and time-dependent GRs be accurately determined from observations. The literature includes many reports of observed GRs, but uncertainties in reported values are typically not well understood. Because it is usually not possible to measure the growth of individual particles as they undergo chemical transformations, GRs are calculated indirectly using time-dependent observations of aerosol properties such as number distributions or number concentrations larger than a given minimum size. Those properties are typically affected by many processes, some poorly understood, that can affect reported GRs to an unknown extent.

A variety of approaches have been used to extract GRs from observations. We refer to these values as GR_m, where the subscript 'm' designates 'measured'. Methods that we discuss include:

1. *Maximum Concentration Method (Kulmala et al., 2012)*. During a nucleation event, particle concentrations in a given size bin increase from their initial values, passing through a peak before they eventually decrease. This

technique involves noting the times that this maximum occurred in two different size bins. The growth rate is then assumed equal to the difference in bin size divided by the difference in time.

2. *Appearance Time Method (Lehtipalo 2014)*. This approach has been used primarily to analyze data from condensation particle counter (CPC) batteries. In brief, GR_m is determined by the differences in concentration rise times (typically, either 5% or 50% of the maximum) measured by CPCs with differing minimum detection sizes. A variation of this approach was reported by Weber et al. (Weber et al., 1997), who estimated growth rates from the observed time delay in measurements of sulfuric acid vapor and particles measured with a condensation particle counter having a minimum detectable size of about 3 nm.

3. *Log-normal Distribution Function Method (Kulmala et al., 2012)*. Lognormal distributions are fit to the growing mode of nucleated particles. GR_m is defined as the growth rate of the geometric mean size of these distributions.

While these methods do not account for the effects of coagulation on measured changes in particle size, the literature includes approaches that explicitly account for such effects (Lehtinen et al., 2004;Verheggen and Mozurkewich, 2006;Kuang et al., 2012;Pichelstorfer et al., 2017). Other work has applied the above techniques after confirming that coagulation has an insignificant effect for the analyzed data (Kulmala et al., 2012) or explicitly accounting for the effects of coagulation on GR_m (Stolzenburg et al., 2005;Lehtipalo et al., 2016).

Recent work has focused on understanding processes that affect *GR* of freshly nucleated atmospheric nanoparticles. This is important because a particle's survival probability increases with *GR* (McMurry and Friedlander, 1979;Weber et al., 1997;Kerminen and Kulmala, 2002;Kuang et al., 2010). Nucleated particles are more likely to form cloud condensation nuclei and affect climate when survival probabilities are high.

This paper assesses errors in GR_m calculated using techniques commonly employed in the literature. Our results are especially germane to *GR* of freshly nucleated particles ranging in size from molecular clusters to about 50 nm. We use time-dependent distribution functions calculated numerically by McMurry and Li (McMurry and Li, 2017) as "data". We do not examine errors associated with convection, source emission, etc. Because we understand this model system perfectly, true particle growth rates (GR_{true}) can be calculated exactly. Errors in GR_m are given by the difference between GR_{true} and GR_m.

We are not the first to examine factors that cause GR_m to differ from GR_{true}. For example, Kontkanen (2016) used simulations to show that discrepancies between GR_m and GR_{true} can be significant. Our approach, which uses the non-dimensional formulation described by McMurry and Li (McMurry and Li, 2017), provides results that are generally applicable to nucleation and growth of a single chemical species, so long as it is being produced by chemical transformations at a constant rate, *R*. We show that the upper limit for errors in GR_m occur when nucleation takes place in the absence of pre-existing aerosols and is collision-controlled (i.e., when evaporation rates from even the smallest clusters occur at rates that are negligible relative to vapor condensation rates). Collision-controlled nucleation is an important limiting case because there is growing evidence that atmospheric nucleation of sulfuric acid with stabilizing species is well-described as a collision-controlled process (Almeida et al., 2013;Kürten et al.,

Atmos. Chem. Phys. Discuss., https://doi.org/10.5194/acp-2018-260
Manuscript under review for journal Atmos. Chem. Phys.
Discussion started: 26 March 2018

Atmospheric Chemistry and Physics Discussions

2018;McMurry, 1980). Because cluster evaporation, scavenging by preexisting aerosol, etc., all diminish the number of particles formed by nucleation, errors in GR_m due to coagulation decrease as these processes gain in prominence. We do not explicitly study the effect of growth by processes other than condensation or evaporation, such as heterogeneous growth pathways that take place on or within existing particles. If such processes were to contribute significantly to growth, they would lead to higher growth rates and therefore smaller relative errors in GR_m due to coagulation. Our results help to inform estimates of uncertainty for complex aerosol systems, such as the atmosphere, where errors are difficult to quantify.

2 Methods

2. 1 Discrete-sectional model

We utilize the dimensionless discrete-sectional model described by McMurry and Li (McMurry and Li, 2017) to simulate evolution of particle size distribution for a system with a single condensing species. We assume that the condensing species is produced at a constant rate by gas phase reaction. Our code uses two hundred discrete bins and 250 sectional bins, with a geometric volume amplification factor of 1.0718 for neighboring sections.

Physical processes that affect particle growth, including wall deposition, loss to pre-existing particles, cluster evaporation and dilution, can be characterized by dimensionless parameters in this model. In the present study, however, not all aforementioned processes are discussed. Our previous work shows that wall losses, scavenging by preexisting particles and dilution have qualitatively similar effects on aerosol dynamics. Therefore, in this work we focus on preexisting aerosols to illustrate factors that contribute to errors in measured growth rates, and do not explicitly discuss wall deposition or dilution. A single dimensionless parameter, $\sqrt{L}$, is used to indicate the abundance of preexisting particles, with larger $\sqrt{L}$ representing higher concentration of preexisting particles (or, equivalently, a slower rate at which the nucleating species is produced by chemical reaction). In addition, we consider the effect of cluster evaporation on particle growth with the assumption that evaporation follows the classical droplet model. Two dimensionless parameters, E and Ω, are needed to fully describe the evaporation process. The dimensionless evaporation parameter, E, is proportional to the saturation vapor concentration of the nucleating species, while Ω is the dimensionless surface tension (McMurry and Li, 2017). To simplify our discussion, Ω is fixed to be 16 throughout this work (a representative value for the surface tension of sulfuric acid aqueous solutions), while the value of E is varied.

The dimensionless simulation results presented here can be converted to dimensional values with the following equations,

$$N_k = \left(\frac{R}{\beta_{11\,fm}}\right)^{1/2} \tilde{N}_k \,;\; t = \left(\frac{1}{R\beta_{11\,fm}}\right)^{1/2} \tau \,;\; d_p = \left(v_1^{1/3}\right)\tilde{d}_p. \quad (3)$$

In the above equations, R is the condensing species production rate, $\beta_{11\,fm}$ is the free molecular collision frequency between 2 monomers, $\tilde{N}_k$ is the dimensionless concentration of particle containing k monomers, τ is the dimensionless time, $\tilde{d}_p$ is the dimensionless particle size and v_1 is the monomer volume. Assuming a monomer

Atmos. Chem. Phys. Discuss., https://doi.org/10.5194/acp-2018-260
Manuscript under review for journal Atmos. Chem. Phys.
Discussion started: 26 March 2018

Atmospheric Chemistry and Physics Discussions

volume of 1.62×10^{-22} cm^3 (volume of one sulfuric acid plus one dimethylamine molecule with a density of 1.47g/cm^3), $\tilde{d}_p = 30$ would be equivalent to a dimensional particle size of 16.4 nm.

2.2 Evaluation of measured growth rate (GR_m)

At time t_1 and t_2, if two particle sizes $d_{p,t1}$ and $d_{p,t2}$ are used to represent the particle size distribution, the 'measured' growth rate can be calculated using the following equation as a first order approximation

$$GR_m\left(\frac{d_{p,t_1}+d_{p,t_2}}{2}, \frac{t_2+t_1}{2}\right) = \frac{d_{p,t_2}-d_{p,t_1}}{t_2-t_1}. \quad (4)$$

If d_{p,t_i} is available for a time series $\{t_i\}_{i=1,2,\ldots}$, growth rate can also be obtained by derivatizing a fitting function $d_p = d_p(t)$ to obtain growth rate at any time t_a:

$$GR_m(d_p, t_a) = \left.\frac{dd_p(t)}{dt}\right|_{t=t_a}. \quad (5)$$

To implement Eq. (4) or (5), it is necessary to choose a particle size that is representative of the particle size distribution at a given time. The choice of this representative size varies among publications and can depend on the types of available data. Based on previous studies (Kulmala et al., 2012;Lehtipalo 2014;Stolzenburg et al., 2005;Yli-Juuti, 2011), we have selected four representative sizes for discussion: $\tilde{d}_{p,mode}$, $\tilde{d}_{p,sr100}$, $\tilde{d}_{p,sr50}$ and $\tilde{d}_{p,tot50}$. At a given time τ, $\tilde{d}_{p,mode}$ is the particle size at which $d\tilde{N}(\tau)/dlog_{10}\tilde{d}_p$ reaches its local maximum. If the shape of the mode is log-normal, $\tilde{d}_{p,mode}$ is equal to the geometric mean of the distribution. As suggested by Kulmala et al. (Kulmala et al., 2012), the 'log-normal distribution method' involves calculating growth rates from observed time-dependent trends of $\tilde{d}_{p,mode}$. The 'maximum concentration method' is based on the time when particles in a given size bin, $\tilde{d}_{p,sr100}$, pass through their maximum (100%) concentration (Lehtinen and Kulmala, 2003). The 'appearance time' method is based on the time when particle concentrations in a bin, $\tilde{d}_{p,sr50}$, pass through a specified percentage of its maximum (we have used 50%). Growth rates are sometimes based on total concentrations of particles larger than a specified size. We refer to the particle size above which the total number concentration of particles reaches 50% of its maximum value as $\tilde{d}_{p,tot50}$. This approach is especially useful when measurements are carried out with a battery of CPCs having differing cutoff sizes. For simplicity, in this paper we assume that CPC detection efficiencies increase from 0% to 100% at a given cutoff size. In practice, measured size-dependent detection efficiencies are typically used when analyzing CPC battery data. Figure 1 shows the location of these representative sizes at $\tau = 20, 60, 100$ for two nucleation scenarios in the absence of preexisting particles. $\tilde{d}_{p,mode}$, $\tilde{d}_{p,sr100}$, $\tilde{d}_{p,sr50}$ and $\tilde{d}_{p,tot50}$ are marked as points, with their y-coordinates representing particle concentrations at corresponding sizes.

As will be shown later, values of GR_m obtained with $\tilde{d}_{p,mode}$, $\tilde{d}_{p,sr100}$, $\tilde{d}_{p,sr50}$ or $\tilde{d}_{p,tot50}$ are not equal. To differentiate these cases, GR_m are notated as $GR_{m,mode}$, $GR_{m,sr100}$, $GR_{m,sr50}$ and $GR_{m,tot50}$ accordingly.

Atmos. Chem. Phys. Discuss., https://doi.org/10.5194/acp-2018-260
Manuscript under review for journal Atmos. Chem. Phys.
Discussion started: 26 March 2018

Atmospheric Chemistry and Physics Discussions

2.3 Evaluation of true growth rate (GR_{true})

The true net growth rate GR_{true}, due to molecular condensation and evaporation, is calculated with the following expression:

$$GR_{true} = \frac{d\tilde{d}_p}{d\tau} = \frac{2}{\pi\tilde{d}_p^2}\frac{d\tilde{V}}{d\tau} = \frac{2}{\pi\tilde{d}_p^2}\cdot\frac{\tilde{V}+c(i,k)\tilde{N}_1\cdot d\tau - E_k\cdot d\tau - \tilde{V}}{d\tau} = \frac{2(c(i,k)\tilde{N}_1 - E_k)}{\pi\tilde{d}_p^2}, \quad (6)$$

where $\tilde{d}_p$ is the representative size, $\tilde{N}_1$ is the concentration of monomers, $c(i,k)$ is the collision frequency between monomers and particles of size $\tilde{d}_p$(containing k monomers), and E_k is the particle the evaporation rate. Assuming cluster evaporation follows the liquid droplet model, E_k is calculated with a discretized equation of the form:

$$E_k = Ec_{1k}\exp\left[\frac{3}{2}\Omega\left(k^{\frac{2}{3}} - (k-1)^{\frac{2}{3}}\right)\right], \quad (7)$$

where Ω is dimensionless surface tension.

If evaporation is negligible ($E_k = 0$) and $\tilde{N}_1$ is constant, Eq. (6) leads to a higher growth rate for smaller particles, mainly because of the increased monomer collision frequency relative to particle size (Tröstl et al., 2016). Throughout this work Eq. (6) is used to evaluate true particle growth rate. Note GR_{true} is calculated from dimensionless size and time, and is therefore dimensionless. Since we focus on relative values of true and measured growth rates, our conclusions are unaffected by the dimensionality of *GR*. However, dimensionless growth rates can be converted to dimensional values with Eq. (3).

3. Results and discussion

3.1 Error of using $GR_{m,mode}$ as GR_{true}

As mode diameter ($\tilde{d}_{p,mode}$) is often employed to derive particle growth rate, in this section we discuss the error of using $GR_{m,mode}$ as a substitute for GR_{true} in the absence of preexisting particles. The effect of preexisting particles is discussed in Sect. 3.3.

Both condensation and coagulation lead to growth of $\tilde{d}_{p,mode}$. To understand their relative importance, we attribute $GR_{m,mode}$ to three processes: monomer condensation minus evaporation (GR_{true}), coagulation of the mode with clusters ($GR_{m,cluster}$) and self-coagulation of the mode ($GR_{m,self}$). The latter two processes are the main causes of the discrepancy between $GR_{m,mode}$ and GR_{true}. To evaluate $GR_{m,cluster}$ and $GR_{m,self}$, the range of 'clusters' and 'mode' are defined as illustrated in Fig. 1 by the two shaded regions at $\tau = 100$: clusters (beige) and nucleation mode (light blue). Clusters and nucleation mode are separated by $\tilde{d}_{p,min}$, where $d\tilde{N}/dlog_{10}\tilde{d}_p$ is at a local minimum. Stolzenburg et al. (Stolzenburg et al., 2005) assumed the nucleation mode is lognormal and calculated GR_{true} and $GR_{m,self}$ with the method of moments. In this work, since the mode for collsion-controlled nucleation deviates significantly from log-normal (see Fig. 1a), no assumption regarding the shape of the nucleation mode is made. Instead, $GR_{m,clsuter}$, $GR_{m,self}$ are calculated with the first order numerical approximation method outlined in Appendix A.

Atmos. Chem. Phys. Discuss., https://doi.org/10.5194/acp-2018-260
Manuscript under review for journal Atmos. Chem. Phys.
Discussion started: 26 March 2018

Atmospheric Chemistry and Physics Discussions

184 The calculation results are summarized by Fig. 2. We first consider collision-controlled nucleation (E=0). For this
185 nucleation scenario, Fig. 2a shows $\tilde{d}_{p,mode}$ on the left y axis and growth rate values on the right. A third order
186 polynomial is used for fitting $\tilde{d}_{p,mode} = \tilde{d}_{p,mode}(\tau)$ and is plotted as a solid black line. Differentiating the fitted
187 polynomial with respect to time gives the value of $GR_{m,mode}$. It is clear that GR_{true} only accounts for a small fraction
188 (17% ~20%) of GR_m and is on par with contribution of $GR_{m,cluster}$ (15%~22%). Self-coagulation is the major
189 contributor (62%~78%) to GR_m. Thus, using $GR_{m,mode}$ as a substitute for GR_{true} leads to an overestimation by as
190 much as a factor about 6. We believe collision-controlled nucleation (E=0) in the absence of other particle loss
191 mechanisms such as wall deposition (W=0) and scavenging by pre-existing particles ($\sqrt{L}$=0) provides an upper limit
192 to errors in GR_m for a constant rate system (R=constant). This is because these conditions lead to the maximum
193 number of particles that can be produced by nucleation. High concentrations lead to high coagulation rates, and it is
194 coagulation that is primarily responsible for errors in GR_m. Furthermore, as is discussed below, the absence of
195 evaporation and scavenging by nucleated particles keeps monomer concentrations low relative to values achieved
196 when E≠0 (see Fig. 2a). Low monomer concentrations reduce the value of GR_{true}, thereby increasing relative errors
197 in GR_m.

198 Distinctive features of particle growth emerge when cluster evaporation is included by setting $E = 1\times10^{-3}$. Figure
199 2b shows results for this nucleation scenario. Most noticeably, particles grow considerably faster at early stages of
200 simulation. To capture this rapid growth, two third-order polynomials are used to fit $\tilde{d}_{p,mode}$ values for $\tau < 40$ and
201 $\tau > 35$ respectively, with an overlapping region for $35 < \tau < 40$. Furthermore, in comparison to collision-
202 controlled nucleation, contribution of $GR_{m,cluster}$ to $GR_{m,mode}$ becomes negligible, due to decreased cluster
203 concentration by evaporation. For $\tau > 30$, GR_{true} accounts for about 40%~55% of $GR_{m,mode}$, larger than that of
204 collision-controlled nucleation; for $\tau < 25$, GR_{true} almost entirely accounts for $GR_{m,mode}$ and even exceeds $GR_{m,mode}$ at
205 the very beginning of the nucleation. $GR_{true}/GR_{m,mode}$>1 indicates a rapidly forming nucleation mode, where freshly
206 nucleated particles enter the mode and skew the mode distribution toward smaller sizes, slowing down the shift of
207 the mode peak towards larger values.

208 Increase of $GR_{true}/GR_{m,mode}$ by evaporation is explained by the elevated monomer concentration due to particle
209 volatility and the smaller number of particles formed by nucleation: the former increases GR_{true}, and the latter
210 decreases $GR_{m,self}$ and $GR_{m,cluster}$. Figure 2c plots monomer concentration $\tilde{N}_1$ as a function of time for several values
211 of E. Noticeably, monomer concentration elevates with E since higher cluster evaporation rates require higher
212 monomer concentrations (i.e., higher supersaturation) to overcome the energy barrier of nucleation. Once nucleation
213 takes place, high monomer concentration leads to rapid nanoparticle growth rates.

214 Figure 2d shows $GR_{true}/GR_{m,mode}$ at $\tau = 30, 50, 100, 150$ for several E values. At a given time, $GR_{true}/GR_{m,mode}$
215 clearly increases with of E: when evaporation rates are not negligible (i.e., E≠0), $GR_{m,mode}$ is closer to GR_{true} than
216 occurs when E=0. Again, this is because the elevated monomer concentrations increase GR_{true} and the lowered
217 concentrations of clusters and nucleated particles decrease $GR_{m,cluster}$ and $GR_{m,self}$. As E approaches 0, the value of
218 $GR_{true}/GR_{m,mode}$ converges to that of the collision-controlled nucleation (~0.2). One data point, corresponding to E =

Atmos. Chem. Phys. Discuss., https://doi.org/10.5194/acp-2018-260
Manuscript under review for journal Atmos. Chem. Phys.
Discussion started: 26 March 2018

Atmospheric Chemistry and Physics Discussions

219 5×10^{-3} and $\tau = 30$, with a value of 1.8, is not shown in Fig. 2d. It has a value significantly greater than unity
220 because of the large quantities of nucleated particles entering the mode, skewing the mode peak toward smaller sizes.

221 **3.2 Comparison of representative sizes**

222 In this section we examine how observed growth rate depends on the choice of a representative size. The application
223 of $GR_{m,mode}$ to deduce GR_{true}, though convenient in practice, depends on the existence of a nucleation mode.
224 However, the nucleation mode is usually not well defined in the early stage of nucleation. In contrast, growth rate
225 based on other representative sizes ($\tilde{d}_{p,sr50}$, $\tilde{d}_{p,sr100}$ and $\tilde{d}_{p,tot50}$) are not dependent on mode formation and are
226 available for all particle sizes. In light of this, $GR_{m,sr100}$, $GR_{m,sr50}$, $GR_{m,tot50}$ have often been employed to describe the
227 growth rate of small particles (<5nm). The effect of pre-existing particles is neglected here (i.e., $\sqrt{L} = 0$) but will be
228 discussed in Sect. 3.3.

229 For collision-controlled nucleation, $\tilde{d}_{p,mode}$, $\tilde{d}_{p,sr50}$, $\tilde{d}_{p,sr100}$, $\tilde{d}_{p,tot50}$ are plotted as functions of time in Fig. 3a.
230 The magnitude of the representative sizes follow $\tilde{d}_{p,mode} < \tilde{d}_{p,bin100} < \tilde{d}_{p,tot50} < \tilde{d}_{p,bin50}$, as was previously
231 illustrated in Fig. 1a. $\tilde{d}_{p,mode} < \tilde{d}_{p,bin100}$ indicates a certain measurement bin first reaches its maximum
232 concentration and becomes a local maximum at a later time. This is true for collision-controlled nucleation with a
233 decreasing peak concentration but is not necessarily true for other nucleation scenarios. The observed growth rate
234 (i.e. slope of curves in Fig. 3a) are shown in Fig. 3b as a function of representative size, with a clear relationship
235 $GR_{m,mode} < GR_{m,sr100} < GR_{m,tot50} < GR_{m,sr50}$. Note that $GR_{m,mode}$ is not available for small sizes, indicating the nucleation
236 mode is yet to form at the early stage of nucleation. Figure 3c shows GR_{true}/GR_m as a function of representative size,
237 with GR_{true} calculated with Eq. (6). Clearly GR_{true} accounts for the highest percentage of GR_m at the start of
238 nucleation. This is partly due to higher monomer concentrations (see red solid curve in Fig. 2c) and partly due to Eq.
239 (6) that leads to higher true growth rate for smaller particles.

240 Figure 3d-3f are counterparts of Fig. 3a-3c, but with evaporation constant E set to 1×10^{-3}. Figure 3d shows rapid
241 increase of representative size with time at the start of nucleation, but a careful examination of clusters containing a
242 few monomers reveals they grow relatively slowly (see the amplified figure at the lower right corner of Fig. 3a. For
243 reference, the dimensionless sizes of monomer, dimer and trimer are 1.24, 1.56 and 1.79 respectively). This reflects
244 that nucleation occurs with a burst of particle formation following a process of monomer and cluster accumulation.
245 The slow growth of the smallest clusters is an indication that the accumulation process is 'slow' due to the strength
246 of the Kelvin effect.

247 Figure 3e shows GR_m obtained by curve fitting after the nucleation burst and Fig. 3f shows the corresponding
248 GR_{trure}/GR_m values. Different from collision-controlled nucleation, there is a sharp rise of GR_{trure}/GR_m value at the
249 start of nucleation. This is due to the sharp decrease of the evaporation term in Eq. (6), causing the value of GR_{true}
250 to increase sharply. As nucleation progresses, the ratio of GR_{true} to $GR_{m,sr100}$, $GR_{m,tot50}$ and $GR_{m,sr50}$ comes close to 1,
251 with $GR_{m,mode}$ not yet available. Eventually, GR_{true}/GR_m for all representative sizes decreases and fall into the range
252 of 30%~50%, with GR_m^{mode} giving the best estimate of GR_{true}. Note the value of $GR_{true}/GR_{m,mode}$ significantly

Atmos. Chem. Phys. Discuss., https://doi.org/10.5194/acp-2018-260
Manuscript under review for journal Atmos. Chem. Phys.
Discussion started: 26 March 2018

Atmospheric Chemistry and Physics Discussions

exceeds unity for $\tilde{d}_p \in [10,15]$ due to the distortion of the mode toward smaller sizes by high flux of freshly nucleated particles into the mode.

3.3 Effect of pre-existing particles

Pre-existing particles act as particle sinks to decrease the intensity of nucleation. Similarly, in chamber experiments, though loss to pre-existing particles is often eliminated by using air that is initially particle-free, loss of particles to chamber walls is inevitable. Since wall loss and loss to preexisting particles have qualitatively similar effect on nucleation (McMurry and Li, 2017), we selectively examine the effect of preexisting particles on growth rate measurements to qualitatively illustrate the effects of all of these processes. To probe the initial stage of nucleation, we use $\tilde{d}_{p,bin50}$ as the basis for our analysis, with a comparison of representative sizes presented at the end of this section. As to the magnitude of $\sqrt{L}$, we choose $\sqrt{L} \in [0,0.3]$ based on previous work. It was shown in Fig. 2b in McMurry and Li (McMurry and Li, 2017) that as $\sqrt{L}$ exceeds 0.1, particle size distributions begin to deviate discernably from the collision-controlled case. In addition, $\sqrt{L} \approx 0.2$ was observed in the ANARChE field campaign carried out in Atlanta for nucleation events with sulfuric acid as the major nucleating species (Kuang et al., 2010).

The influence of preexisting particles on the discrepancy between true and measured growth rate (GR_{true}/GR_m) is twofold. On one hand, preexisting particles can decrease monomer concentration which leads to a smaller GR_{true}. On the other hand, preexisting particles reduces coagulation by scavenging nucleated particles, which results in a narrower gap between GR_{true} and GR_m. Therefore, the response of GR_{true}/GR_m to $\sqrt{L}$ depends on the relative magnitude of these two competing effects. Figure 4a shows $\tilde{d}_{p,sr50}$ as a function of time for several $\sqrt{L}$ values and Fig. 4b displays the corresponding GR_{true}/GR_m values. It can be seen that GR_{true}/GR_m positively correlates with $\sqrt{L}$, indicating preexisting particles is more effective in removing nucleated particles than reducing monomer concentrations. In fact, as further demonstrated by Fig. 4c, monomer concentrations (leftmost point of all the curves) are barely affected: scavenging of monomers by preexisting particles are offset by less condensation onto nucleated particles. Note for the range of $\sqrt{L}$ values examined, the presence of preexisting particles alter GR_{true}/GR_m values by no more than 50%.

Figure 4d-4f show the same quantities as are shown in Fig. 4a-4c, but with E set to 1×10^{-3} instead of zero. In contrast to collision-controlled nucleation, pre-existing particles significantly affect the nucleation process when cluster evaporation is taken into account. As $\sqrt{L}$ increases, Fig. 4e shows GR_{true}/GR_m converges to a value slightly larger than unity. This indicates that the contribution of coagulation to measured growth rate approaches zero as $\sqrt{L}$ becomes large; or equivalently, the concentration of nucleated particles is severely decreased by pre-existing particles. Values of $GR_{true}/GR_{m,sr50}$ slightly exceed unity for large sizes (Fig. 4f) due to the slightly higher condensational growth rates of smaller particles in the nucleation mode. This shifts values of $\tilde{d}_{p,sr50}$ towards smaller sizes than would occur if all particles were to grow at the same rate, causing $GR_{m,sr50}$ to be smaller than GR_{true}.

The decrease of nucleated particle concentration is further demonstrated in Fig. 4f. From $\sqrt{L} = 0$ to $\sqrt{L} = 0.3$, the peak concentration of nucleated particles dropped by about three orders of magnitude. Such a decrease in concentration of nucleated particles results from the limiting effect of $\sqrt{L}$ on monomer concentration at the moment of the nucleation burst. If pre-existing particles are absent, then no major loss mechanisms for monomers exist prior to nucleation burst. Monomer would accumulate until the nucleation energy barrier can be overcome: the higher the energy barrier, the higher the monomer concentration accumulates to be (shown in Fig. 2c). The elevated monomer concentration then leads to rapid growth of freshly nucleated particles right after nucleation burst. However, in the presence of pre-existing particles (i.e., $\sqrt{L} \neq 0$), monomer concentration can only increase to the point where its production and consumption by preexisting particles reach balance, prohibiting its concentration from reaching a high value even prior to nucleation burst.

Finally, Fig. 5 examines the difference between representative sizes used to calculate GR_m when loss to preexisting particles is accounted for. Two cases are presented: (1) collision-controlled nucleation with $\sqrt{L} = 0.2$ (Fig. 5a-5c) and (2) nucleation with evaporation constant $E = 1\times10^{-3}$ & $\sqrt{L} = 0.2$ (Fig. 5d-5f). For collision-controlled nucleation, such a concentration ($\sqrt{L} = 0.2$) of preexisting particles changes nucleation only slightly. Though GR_m decreases and GR_{true}/GR_m increases both to a minor extent compared to collision-controlled nucleation (compare Fig. 5a-5c to Fig. 3a-3c), the analysis made in the discussion of Fig. 3a-3c still stands for Fig. 5a-5c.

For nucleation with evaporation and preexisting particles coupled together, two features are worthy of attention. Firstly, compared to evaporation-only nucleation, GR_m is significantly decreased for small particle sizes. For $\tilde{d}_p < 10$, GR_m is no larger than 0.7 with preexisting particles but can be greater than 1.5 without (refer to Fig. 3e). Secondly, as shown in Fig. 5f, GR_{true}/GR_m comes close to unity for all representative sizes due to negligible coagulation effects. In practice, this means measured growth rate based on all the four representative sizes can be a reasonable substitute of the true growth rate in a similar nucleation scenario.

4 Conclusions

We used a discrete-sectional model to solve a dimensionless form of aerosol population balance equation for a single-species system. True growth rate and various "measured" growth rates were examined for a variety of nucleation scenarios. Based on the simulation results, we draw the following conclusions:

1. Collision-controlled nucleation without preexisting particles results in an upper limit (up to a factor of 6) to discrepancies between true (GR_{true}) and measured (e.g., $GR_{m,mode}$) growth rates.
2. In the absence of preexisting particles, comparison of different growth rates based on different representative sizes indicates the relationship $GR_{m,mode}<GR_{m,sr100}<GR_{m,tot50}<GR_{m,sr50}$ holds true for collision-controlled nucleation. If clusters evaporate, the nucleation process is characterized by rapid particle growth following nucleation burst.

3. Both evaporation and preexisting particles bring GR_{true}/GR_m closer to unity by decreasing the number of nucleated particles. In the case of evaporation, GR_{true}/GR_m also increases as a result of elevated monomer concentration.
4. Preexisting particles have dramatically different effects on collision-controlled nucleation and nucleation with cluster evaporation. For $\sqrt{L} \in [0,0.3]$, collision-controlled nucleation is only slightly affected. However, if preexisting particles are coupled with evaporation, the number of nucleated particles can drop significantly. In this case, GR_m based on all representative sizes can be a good approximation of GR_{true} due to negligible coagulation effects.

Atmos. Chem. Phys. Discuss., https://doi.org/10.5194/acp-2018-260
Manuscript under review for journal Atmos. Chem. Phys.
Discussion started: 26 March 2018

Atmospheric Chemistry and Physics Discussions

Appendix A

To evaluate the contribution of self-coagulation of the mode ($GR_{m,self}$) and cluster coagulation ($GR_{m,clsuter}$) to measured growth rate based on mode diameter ($GR_{m,mode}$), we used the following first order numerical approximation method:

1. Find particle size distribution $\tilde{n} = \tilde{n}(k,\tau)$ at a given time τ. k is the number of monomers in a particle and $\tilde{n}_k$ is the concentration of particles that contains k molecules. Since the simulation code only reports discrete particle concentration for each bin, an interpolation is performed using Matlab function *griddedInterpolant.m*.
2. Find the value $k = k_{max}$ at which $3\log(10)\,k\tilde{n}(k,\tau)$ is locally maximized. A prefactor $3\log(10)\,k$ is multiplied to $\tilde{n}(k,\tau)$ to convert the particle size distribution to $d\tilde{N}/dlog_{10}\tilde{d}_p$. The mode diameter is then given by $\tilde{d}_{p,mode}(\tau) = \left(\frac{6k_{max}}{\pi}\right)^{1/3}$
3. Use the following integration equations to obtain number distribution of the mode at time $\tau + \Delta\tau$ assuming only one process causes the distribution to shift.

   For self-coagulation:

   $$\tilde{n}_{self}(k,\tau+\Delta\tau) = \tilde{n}(k) + 0.5 * \Delta\tau * \int_L^k c(x,k-x)\tilde{n}(x,\tau)\tilde{n}(k-x,\tau)dx - \int_L^H c(x,k)\tilde{n}(k,\tau)\tilde{n}(x,\tau)dx. \quad \text{(A1)}$$

   For coagulation with clusters:

   $$\tilde{n}_{cluster}(k,\tau+\Delta\tau) = \tilde{n}(k,\tau) + 0.5\cdot\Delta\tau\cdot\int_{L_c}^{H_c} c(x,k-x)\tilde{n}(x,\tau)\tilde{n}(k-x,\tau)H(H_c-k+x)dx + \Delta\tau\cdot$$
   $$\int_{L_c}^{H_c} c(x,k-x)\tilde{n}(x,\tau)\tilde{n}(k-x,\tau)H(k-x-H_c)dx + -\Delta\tau\cdot\int_{L_c}^{H_c} c(x,k)\tilde{n}(x,\tau)\tilde{n}(k,\tau)dx. \quad \text{(A2)}$$

   In the above equations, L and H are the lower and upper boundary of the mode, L_c and H_c are the lower and upper boundary of clusters, $c(i,j)$ is the collision frequency function, *H(x)* is the Heaviside step function. $\Delta\tau$ is typically set between 0.1 to 1.
4. Find the k values at which $3\log(10)\,k\tilde{n}_{self}(k,\tau+\Delta\tau)$ and $3\log(10)\,k\tilde{n}_{cluster}(k,\tau+\Delta\tau)$ are locally maximized. The corresponding diameters are $\tilde{d}_{p,self}(\tau+\Delta\tau)$ and $\tilde{d}_{p,cluster}(\tau+\Delta\tau)$.
5. The growth rate due to self-coagulation and coagulation with clusters are then given by

   $$GR_{m,self} = \frac{\tilde{d}_{p,self}(\tau+\Delta\tau)-\tilde{d}_{p,mode}(\tau)}{\Delta\tau};\ GR_{m,cluster} = \frac{\tilde{d}_{p,cluster}(\tau+\Delta\tau)-\tilde{d}_{p,mode}(\tau)}{\Delta\tau}. \quad \text{(A3)}$$

Acknowledgements

This research was supported by the US Department of Energy's Atmospheric System Research, an Office of Science, Office of Biological and Environmental Research program, under grant number DE-SC0011780.

Nomenclature

Collision-controlled nucleation: a limiting case for nucleation where all collisions between condensing (nucleating) vapor occur at the rate predicted by kinetic theory and particles stick with 100% efficiency. Vapor does not subsequently evaporate from particle surfaces, nor are particles scavenged by pre-existing particles or the chamber wall

$\tilde{d}_{p,min}$: particle size corresponding to the local minimum in a $d\tilde{N}/dlog_{10}\tilde{d}_p$ representation of particle size distribution

$\tilde{d}_{p,mode}$: particle size corresponding to the local maximum in a $d\tilde{N}/dlog_{10}\tilde{d}_p$ representation of particle size distribution

$\tilde{d}_{p,sr50}$: particle size of a measurement bin where particle concentration reaches 50% of its maximum value

$\tilde{d}_{p,sr100}$: particle size of a measurement bin where particle concentration reaches maximum value

$\tilde{d}_{p,tot50}$: particle size above which total particle concentration reaches 50% of its maximum value

$GR_{m,mode}$: measured dimensionless growth rate based on $\tilde{d}_{p,mode}$

$GR_{m,sr50}$: measured dimensionless growth rate based on $\tilde{d}_{p,sr50}$

$GR_{m,sr100}$: measured dimensionless growth rate based on $\tilde{d}_{p,sr100}$

$GR_{m,tot50}$: measured dimensionless growth rate based on $\tilde{d}_{p,tot50}$

GR_{true}: true dimensionless particle growth rate attributed to the net flux of condensing vapors onto particle surface (i.e., the condensation rate minus the evaporation rate)

$GR_{m,clsuter}$: measured dimensionless particle growth rate attributed to coagulation with clusters

$GR_{m,self}$: measured dimensionless growth rate attributed to self-coagulation of particles in the nucleation mode

E, Ω: dimensionless parameters characterizing evaporation rates of particles, derived from the liquid droplet model. E can be regarded as a dimensionless form of saturation vapor pressure of the condensing molecules and Ω a dimensionless form of surface tension. Ω assumes a constant value of 16in this work.

$\sqrt{L}$: dimensionless parameter characterizing fractional loss rate of monomer or nucleated particles to pre-existing particles

$\tilde{N}_k$: dimensionless concentration of particles containing k monomers (i.e., k molecules of condensed vapor)

References

Almeida, J., Schobesberger, S., Kürten, A., Ortega, I. K., Kupiainen-Määttä, O., Praplan, A. P., Adamov, A., Amorim, A., Bianchi, F., Breitenlechner, M., David, A., Dommen, J., Donahue, N. M., Downard, A., Dunne, E., Duplissy, J., Ehrhart, S., Flagan, R. C., Franchin, A., Guida, R., Hakala, J., Hansel, A., Heinritzi, M., Henschel, H., Jokinen, T., Junninen, H., Kajos, M., Kangasluoma, J., Keskinen, H., Kupc, A., Kurtén, T., Kvashin, A. N., Laaksonen, A., Lehtipalo, K., Leiminger, M., Leppä, J., Loukonen, V., Makhmutov, V., Mathot, S., McGrath, M. J., Nieminen, T., Olenius, T., Onnela, A., Petäjä, T., Riccobono, F., Riipinen, I., Rissanen, M., Rondo, L., Ruuskanen, T., Santos, F. D., Sarnela, N., Schallhart, S., Schnitzhofer, R., Seinfeld, J. H., Simon, M., Sipilä, M., Stozhkov, Y., Stratmann, F., Tomé, A., Tröstl, J., Tsagkogeorgas, G., Vaattovaara, P., Viisanen, Y., Virtanen, A., Vrtala, A., Wagner, P. E., Weingartner, E., Wex, H., Williamson, C., Wimmer, D., Ye, P., Yli-Juuti, T., Carslaw, K. S., Kulmala, M., Curtius, J., Baltensperger, U., Worsnop, D. R., Vehkamäki, H., and Kirkby, J.: Molecular understanding of sulphuric acid–amine particle nucleation in the atmosphere, Nature, 502, 359, 10.1038/nature12663

https://www.nature.com/articles/nature12663 - supplementary-information, 2013.

Friedlander, S. K.: Smoke, dust, and haze : fundamentals of aerosol dynamics, 2nd ed.. ed., New York : Oxford University Press, New York, 2000.

Gelbard, F., and Seinfeld, J. H.: The general dynamic equation for aerosols. Theory and application to aerosol formation and growth, Journal of Colloid and Interface Science, 68, 363-382, https://doi.org/10.1016/0021-9797(79)90289-3, 1979.

Gelbard, F., and Seinfeld, J. H.: Simulation of multicomponent aerosol dynamics, Journal of Colloid and Interface Science, 78, 485-501, https://doi.org/10.1016/0021-9797(80)90587-1, 1980.

Heisler, S. L., and Friedlander, S. K.: Gas-to-particle conversion in photochemical smog: Aerosol growth laws and mechanisms for organics, Atmospheric Environment (1967), 11, 157-168, https://doi.org/10.1016/0004-6981(77)90220-7, 1977.

Kerminen, V. M., and Kulmala, M.: Analytical formulae connecting the "real" and the "apparent" nucleation rate and the nuclei number concentration for atmospheric nucleation events, Journal of Aerosol Science, 33, 609-622, 2002.

Kontkanen, J., Olenius, T., Lehtipalo, K., Vehkamäki, H., Kulmala, M., and Lehtinen, K. E. J.: Growth of atmospheric clusters involving cluster–cluster collisions: comparison of different growth rate methods, Atmos. Chem. Phys., 16, 5545-5560, 10.5194/acp-16-5545-2016, 2016.

Kuang, C., Riipinen, I., Yli-Juuti, T., Kulmala, M., McCormick, A. V., and McMurry, P. H.: An improved criterion for new particle formation in diverse atmospheric environments, Atmospheric Chemistry and Physics, 10, 1-12, 10.5194/acp-10-1-2010, 2010.

Kuang, C., Chen, M., Zhao, J., Smith, J., McMurry, P. H., and Wang, J.: Size and time-resolved growth rate measurements of 1 to 5 nm freshly formed atmospheric nuclei, Atmos. Chem. Phys., 12, 3573-3589, 10.5194/acp-12-3573-2012, 2012.

Kulmala, M., Petäjä, T., Nieminen, T., Sipilä, M., Manninen, H. E., Lehtipalo, K., Dal Maso, M., Aalto, P. P., Junninen, H., Paasonen, P., Riipinen, I., Lehtinen, K. E. J., Laaksonen, A., and Kerminen, V.-M.: Measurement of the nucleation of atmospheric aerosol particles, Nature Protocols, 7, 1651, 10.1038/nprot.2012.091

https://www.nature.com/articles/nprot.2012.091 - supplementary-information, 2012.

Kürten, A., Li, C., Bianchi, F., Curtius, J., Dias, A., Donahue, N. M., Duplissy, J., Flagan, R. C., Hakala, J., Jokinen, T., Kirkby, J., Kulmala, M., Laaksonen, A., Lehtipalo, K., Makhmutov, V., Onnela, A., Rissanen, M. P., Simon, M., Sipilä, M., Stozhkov, Y., Tröstl, J., Ye, P., and McMurry, P. H.: New particle formation in the sulfuric acid–dimethylamine–water system: reevaluation of CLOUD chamber measurements and

comparison to an aerosol nucleation and growth model, Atmos. Chem. Phys., 18, 845-863, 10.5194/acp-18-845-2018, 2018.
Lehtinen, K. E. J., and Kulmala, M.: A model for particle formation and growth in the atmosphere with molecular resolution in size, Atmos. Chem. Phys., 3, 251-257, 10.5194/acp-3-251-2003, 2003.
Lehtinen, K. E. J., Rannik, U., Petaja, T., Kulmala, M., and Hari, P.: Nucleation rate and vapor concentration estimations using a least squares aerosol dynamics method - art. no. D21209, Journal of Geophysical Research-Atmospheres, 109, 21209, 2004.
Lehtipalo, K., Rondo, L., Kontkanen, J., Schobesberger, S., Jokinen, T., Sarnela, N., Kürten, A., Ehrhart, S., Franchin, A., Nieminen, T., Riccobono, F., Sipilä, M., Yli-Juuti, T., Duplissy, J., Adamov, A., Ahlm, L., Almeida, J., Amorim, A., Bianchi, F., Breitenlechner, M., Dommen, J., Downard, A. J., Dunne, E. M., Flagan, R. C., Guida, R., Hakala, J., Hansel, A., Jud, W., Kangasluoma, J., Kerminen, V.-M., Keskinen, H., Kim, J., Kirkby, J., Kupc, A., Kupiainen-Määttä, O., Laaksonen, A., Lawler, M. J., Leiminger, M., Mathot, S., Olenius, T., Ortega, I. K., Onnela, A., Petäjä, u., Praplan, A., Rissanen, M. P., Ruuskanen, T., Santos, F. D., Schallhart, S., Schnitzhofer, R., Simon, M., Smith, J. N., Tröstl, J., Tsagkogeorgas, G., Tome, A. n., Vaattovaara, P., Hanna Vehkama¨ki1, Vrtala, A. E., Wagner, P. E., Williamson, C., Wimmer, D., Winkler, P. M., Virtanen, A., Donahue, N. M., Carslaw, K. S., Baltensperger, U., Riipinen, I., Curtius, J., Worsnop, D. R., and Kulmala, M.: The effect of acid-base clustering and ions on the growth of atmospheric nano-particles, Nature Communications, 7, 11594, 2016.
Lehtipalo , K., Leppa , J , Kontkanen , J , Kangasluoma , J , Franchin , A , Wimnner , D , Schobesberger , S , Junninen , H , Petaja , T , Sipila , M , Mikkila , J , Vanhanen , J , Worsnop , D R & Kulmala: Methods for determining particle size distribution and growth rates between 1 and 3 nm using the Particle Size Magnifier, Boreal Environment Research, 19, 215-236, 2014.
McMurry, P. H., and Friedlander, S. K.: New particle formation in the presence of an aerosol, Atmos. Environ., 13, 1635-1651, 1979.
McMurry, P. H.: Photochemical aerosol formation from SO2: A theoretical analysis of smog chamber data, Journal of Colloid and Interface Science, 78, 513-527, https://doi.org/10.1016/0021-9797(80)90589-5, 1980.
McMurry, P. H., and Wilson, J. C.: Growth laws for the formation of secondary ambient aerosols: Implications for chemical conversion mechanisms, Atmospheric Environment (1967), 16, 121-134, https://doi.org/10.1016/0004-6981(82)90319-5, 1982.
McMurry, P. H., and Li, C.: The dynamic behavior of nucleating aerosols in constant reaction rate systems: Dimensional analysis and generic numerical solutions, Aerosol Science and Technology, 51, 1057-1070, 10.1080/02786826.2017.1331292, 2017.
Pichelstorfer, L., Stolzenburg, D., Ortega, J., Karl, T., Kokkola, H., Laakso, A., Lehtinen, K. E. J., Smith, J. N., McMurry, P. H., and Winkler, P. M.: Resolving nanoparticle growth mechanisms from size- and time-dependent growth rate analysis, Atmos. Chem. Phys. Discuss., 2017, 1-24, 10.5194/acp-2017-658, 2017.
Riipinen, I.: The contribution of organics to atmospheric nanoparticle growth, Nat. Geosci., 5, 453-458, 2012.
Stolzenburg, M. R., McMurry, P. H., Sakurai, H., Smith, J. N., Mauldin, R. L., Eisele, F. L., and Clement, C. F.: Growth rates of freshly nucleated atmospheric particles in Atlanta, Journal of Geophysical Research: Atmospheres, 110, n/a-n/a, 10.1029/2005JD005935, 2005.
Tröstl, J., Chuang, W. K., Gordon, H., Heinritzi, M., Yan, C., Molteni, U., Ahlm, L., Frege, C., Bianchi, F., Wagner, R., Simon, M., Lehtipalo, K., Williamson, C., Craven, J. S., Duplissy, J., Adamov, A., Almeida, J., Bernhammer, A.-K., Breitenlechner, M., Brilke, S., Dias, A., Ehrhart, S., Flagan, R. C., Franchin, A., Fuchs, C., Guida, R., Gysel, M., Hansel, A., Hoyle, C. R., Jokinen, T., Junninen, H., Kangasluoma, J., Keskinen, H., Kim, J., Krapf, M., Kürten, A., Laaksonen, A., Lawler, M., Leiminger, M., Mathot, S., Möhler, O., Nieminen, T., Onnela, A., Petäjä, T., Piel, F. M., Miettinen, P., Rissanen, M. P., Rondo, L., Sarnela, N., Schobesberger, S., Sengupta, K., Sipilä, M., Smith, J. N., Steiner, G., Tomè, A., Virtanen, A., Wagner, A. C., Weingartner, E.,

473 Wimmer, D., Winkler, P. M., Ye, P., Carslaw, K. S., Curtius, J., Dommen, J., Kirkby, J., Kulmala, M., Riipinen,
474 I., Worsnop, D. R., Donahue, N. M., and Baltensperger, U.: The role of low-volatility organic compounds
475 in initial particle growth in the atmosphere, Nature, 533, 527, 10.1038/nature18271, 2016.
476 Verheggen, B., and Mozurkewich, M.: An inverse modeling procedure to determine particle growth and
477 nucleation rates from *measured* *aerosol* size distributions, Atmospheric Chemistry and Physics, 6,
478 2927-2942, 2006.
479 Weber, R. J., Marti, J. J., McMurry, P. H., Eisele, F. L., Tanner, D. J., and Jefferson, A.: Measurements of
480 new particle formation and ultrafine particle growth rates at a clean continental site, Journal of
481 Geophysical Research: Atmospheres, 102, 4375-4385, 10.1029/96JD03656, 1997.
482 Yli-Juuti, T.: Growth rates of nucleation mode particles in Hyytiälä during 2003–2009: variation with
483 particle size, season, data analysis method and ambient conditions, Atmos. Chem. Phys., 11, 12865-
484 12886, 2011.

485

Atmos. Chem. Phys. Discuss., https://doi.org/10.5194/acp-2018-260
Manuscript under review for journal Atmos. Chem. Phys.
Discussion started: 26 March 2018

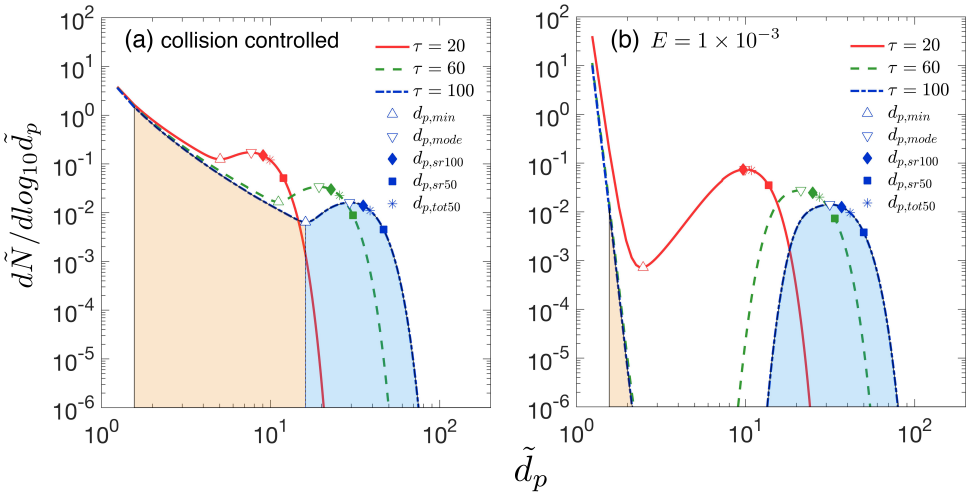

Figure 1. Particle size distributions at dimensionless times $\tau = 20, 60, 100$ **(a)** for collision-controlled nucleation and **(b)** when evaporation is included with $E = 1{\times}10^{-3}$. Division of the distribution into monomer, cluster and nucleation mode is displayed for $\tau = 100$, with beige and light blue indicating the range of clusters and nucleation mode. Characteristic sizes $\tilde{d}_{p,mode}$, $\tilde{d}_{p,sr100}$, $\tilde{d}_{p,sr50}$ and $\tilde{d}_{p,tot50}$ are marked for each time. The relationship between symbols and characteristic sizes is shown only for τ=100.

Atmos. Chem. Phys. Discuss., https://doi.org/10.5194/acp-2018-260
Manuscript under review for journal Atmos. Chem. Phys.
Discussion started: 26 March 2018

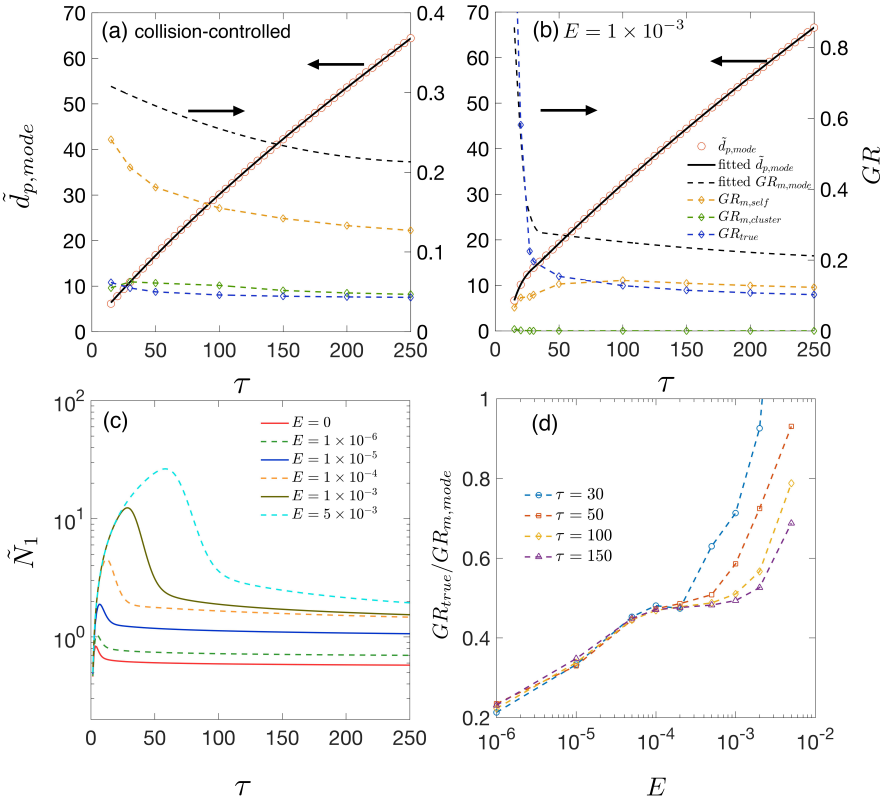

Figure 2. (a) $\tilde{d}_{p,mode}$ and various growth rates as functions of time for collision-controlled nucleation. Dashed black lines show the value of $GR_{m,mode}$. Yellow, green and blue dashed lines represent $GR_{m,self}$, $GR_{m,cluster}$ and GR_{true} respectively. **(b)** The same quantities as are shown in (a) but with the evaporation constant set to $E = 1{\times}10^{-3}$. For both Fig. 2a and 2b, the left axis shows value for the solid lines and the right axis shows values for the dashed lines. **(c)** Monomer concentration as functions of time for different values of E. **(d)** $GR_{true}/GR_{m,mode}$ for different values of E at $\tau = 30, 50, 100, 150$.

Atmos. Chem. Phys. Discuss., https://doi.org/10.5194/acp-2018-260
Manuscript under review for journal Atmos. Chem. Phys.
Discussion started: 26 March 2018

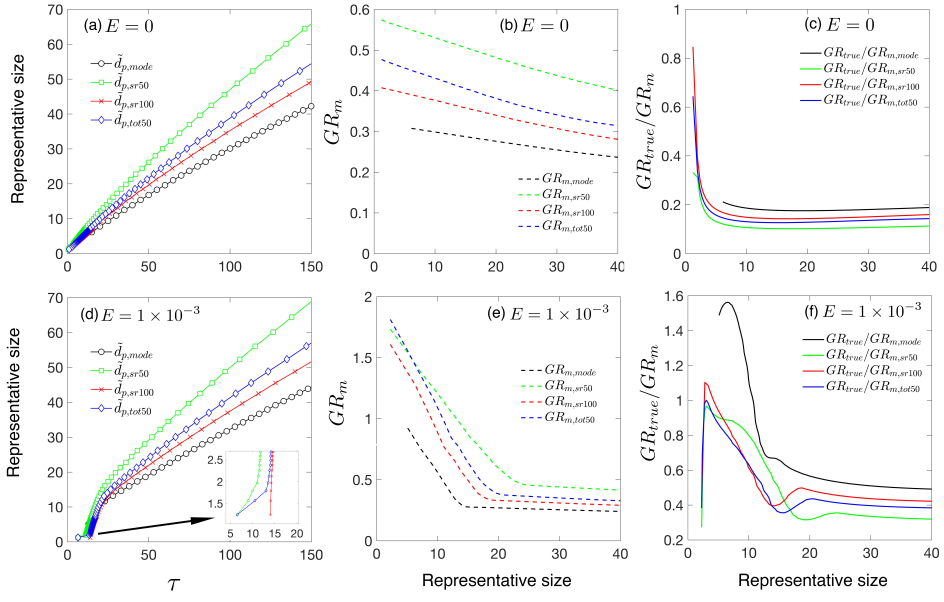

Figure 3. (a) $\tilde{d}_{p,mode}$, $\tilde{d}_{p,sr100}$, $\tilde{d}_{p,tot50}$, $\tilde{d}_{p,bin50}$ as functions of time. **(b)** Measured growth rates $GR_{m,mode}$, $GR_{m,sr50}$, $GR_{m,sr100}$, $GR_{m,tot50}$ as functions of representative sizes. **(c)** Ratio of true growth rate to measured growth rate, GR_{true}/GR_m. Figures 3a-3c are for collision-controlled nucleation with E=0. Figures 3d-3f show the same quantities as are shown in Fig. 3a-3c but with $E = 1\times10^{-3}$.

Atmos. Chem. Phys. Discuss., https://doi.org/10.5194/acp-2018-260
Manuscript under review for journal Atmos. Chem. Phys.
Discussion started: 26 March 2018

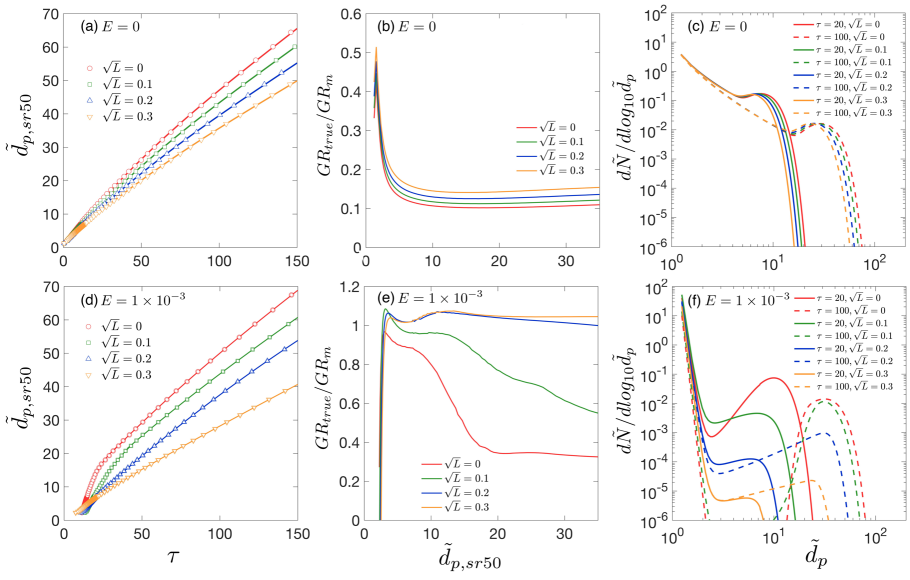

Figure 4. Effect of preexisting particles on particle growth rate. **(a)** $\tilde{d}_{p,sr50}$ as a function of time. **(b)** Ratio of true growth rate to measured growth rate, $GR_{true}/GR_{m,sr50}$. **(c)** Particle size distributions at $\tau = 20$ and $\tau = 100$. Figures 4a-4c are for collision-controlled nucleation with $E = 0$ and $\sqrt{L} = 0, 0.1, 0.2, 0.3$. Figures 4c-4d show the same quantities as are shown in Fig. 4a-4c but with $E = 1{\times}10^{-3}$.

Atmos. Chem. Phys. Discuss., https://doi.org/10.5194/acp-2018-260
Manuscript under review for journal Atmos. Chem. Phys.
Discussion started: 26 March 2018

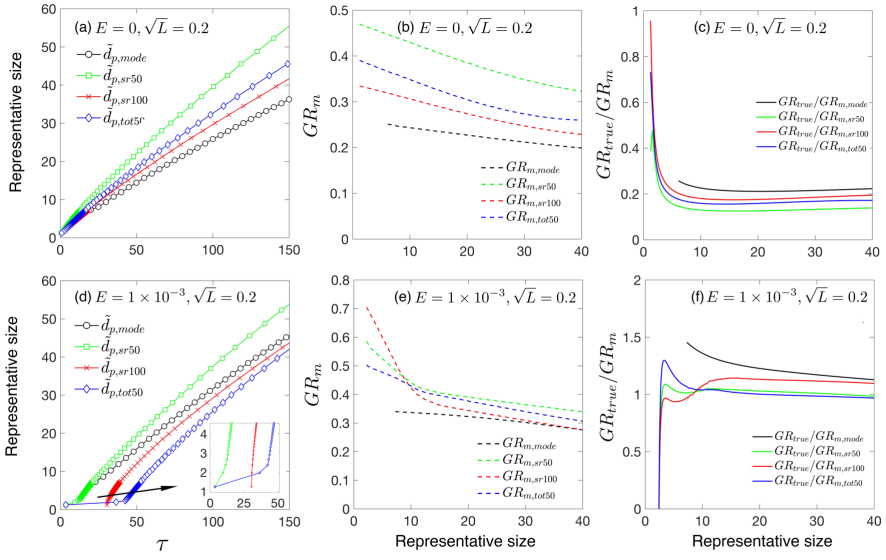

Figure 5. (a) $\tilde{d}_{p,mode}$, $\tilde{d}_{p,sr100}$, $\tilde{d}_{p,tot50}$, $\tilde{d}_{p,bin50}$ as functions of time. **(b)** Measured growth rate $GR_{m,mode}$, $GR_{m,sr50}$, $GR_{m,sr100}$, $GR_{m,tot50}$ as functions of representative sizes. **(c)** Ratio of true growth rate to measured growth rate, GR_{true}/GR_m. Figures 5a-5c are for collision-controlled nucleation with $E = 0$ and $\sqrt{L} = 0.2$. Figures 5d-5f show the same quantities as are shown in Fig. 5a-5c but with $E = 1{\times}10^{-3}$.